

Simulation of the structure and filtration performance of granular porous membranes

G.A. Davies*, X. Jia

Department of Chemical Engineering, UMIST, Manchester M60 1QD, United Kingdom

Received 3 November 1994; accepted 16 March 1995

Abstract

This paper describes a complete simulation package for simulation of granular membranes and membrane filtration/back-flushing processes. It consists of two basic models, one (the sphere packing model) for the structure of granular membranes, and the other (the random network model) for the morphology of the interconnected pores in the membrane media; and procedures to use the generated model structure to simulate filtration/backflushing processes in three distinct cases, namely cake filtration ($a \gg a_p$), internal fouling ($a \gg a_p$) and a transient case ($a \sim a_p$) where both internal fouling and cake build-up are important.

Keywords: Simulation; Structural performance; Filtration performance; Granular porous membranes

1. Introduction

Granular porous media are encountered in many industrial and natural processes such as membrane filtration and ground water migration. Hence the importance of simulation of the structure of porous media and transport phenomena within the media. This paper describes two simulation models for such purposes and demonstrates how the models may be applied to membrane filtration in different modes.

For many practical purposes, it is quite acceptable to use random packing of spheres to represent the structure of granular porous media. The random packing of spheres has long been a subject of extensive study by both theorists and experimentalists from a wide diversity of disciplines for academic interest and practical significance. Consequently, a number of algorithms

exist to generate random packing of spheres [1]. Our *sphere packing model* is based a ballistic algorithm proposed by Vold [2]. The model can be used to simulate the structure of *unconsolidated granular porous media*. With some additional modifications to the generated model structure, the more complex structure of *sintered* or *consolidated granular porous media* can also be obtained.

To study particle transport in the porous media, it is essential to know the flow distribution inside the porous media. However, given the complexity of the problem, it is only feasible to adopt an approximate approach to the problem. The approximation operates at three levels or stages. First, the actual pores are approximated by some geometrically simple or well-defined shapes. The simplest and most commonly used is the cylindrical tube. More sophisticated models are available which use converging–diverging constricted tubes [3], tetrahedrons [4], or rectangular tubes [5] to represent

* Corresponding author. Tel: 0161-200-4342. Fax: 0161-200-4399. E-Mail: G.A.DAVIES@UMIST.AC.UK

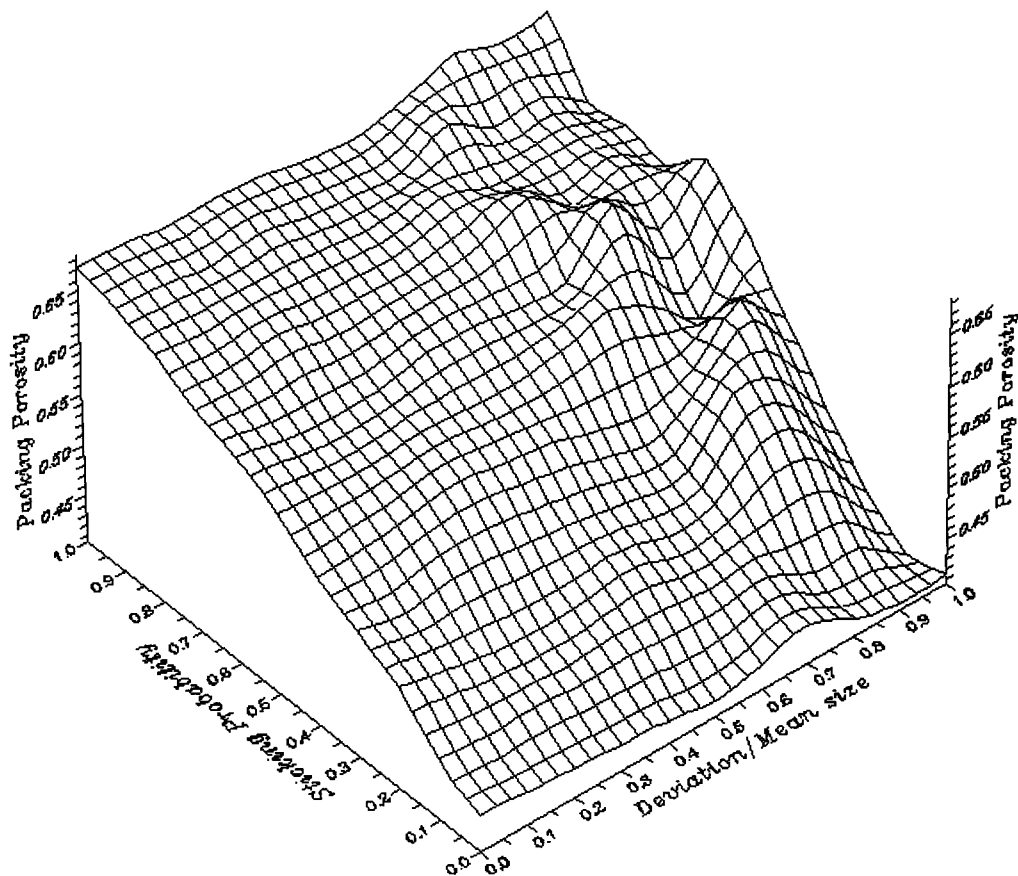


Fig. 1. Packing porosity as a function of sticking probability and size distribution.

the actual pores. However, given the approximate nature of the approach, the more sophisticated models do not necessarily improve the overall accuracy of the simulation results as much as to justify the extra effort needed. Therefore, we have chosen to employ the simple cylindrical-tube representation in our simulations. Secondly, the interconnected pores in the porous medium are modelled by a network of cylindrical tubes (or some other chosen shapes). Both 2D and 3D networks have been employed by various researchers, as reviewed by Dullien [6]. With few exceptions [7,8], all the networks used so far to model the porous media have been built upon a regular, typically a square (2D) or cubic (3D), lattice. There are variations as to whether to consider explicitly the finite volume of nodes in the network [5] or not [9]. And finally, the flow through the porous medium is computed based on the random network, in a manner analogous to the calculation of electrical current in a resistive circuit. It

is worth noting that a disadvantage common to all the network models reported in the aforementioned literature is the lack of a direct morphological link between the network and the actual structure of the porous medium. The *random network model* to be described in this paper has the obvious advantage of being able to provide such a link, through a tessellation algorithm, so that the flow distribution can actually be mapped onto the actual structure of the porous medium.

Once we have the model structure for the porous media and the random network built upon the model structure, we can proceed to simulate the actual filtration and/or backflushing processes. Here, three distinct cases may be distinguished according to the size ratio, $\alpha = a/a_p$, where a is the mean particle radius and a_p is the mean pore size which, in accordance with the model representation, is equivalent to the mean tube radius. If $\alpha \gg 1$ (i.e. the particles are much larger than the average pore size), cake build-up on top of the porous

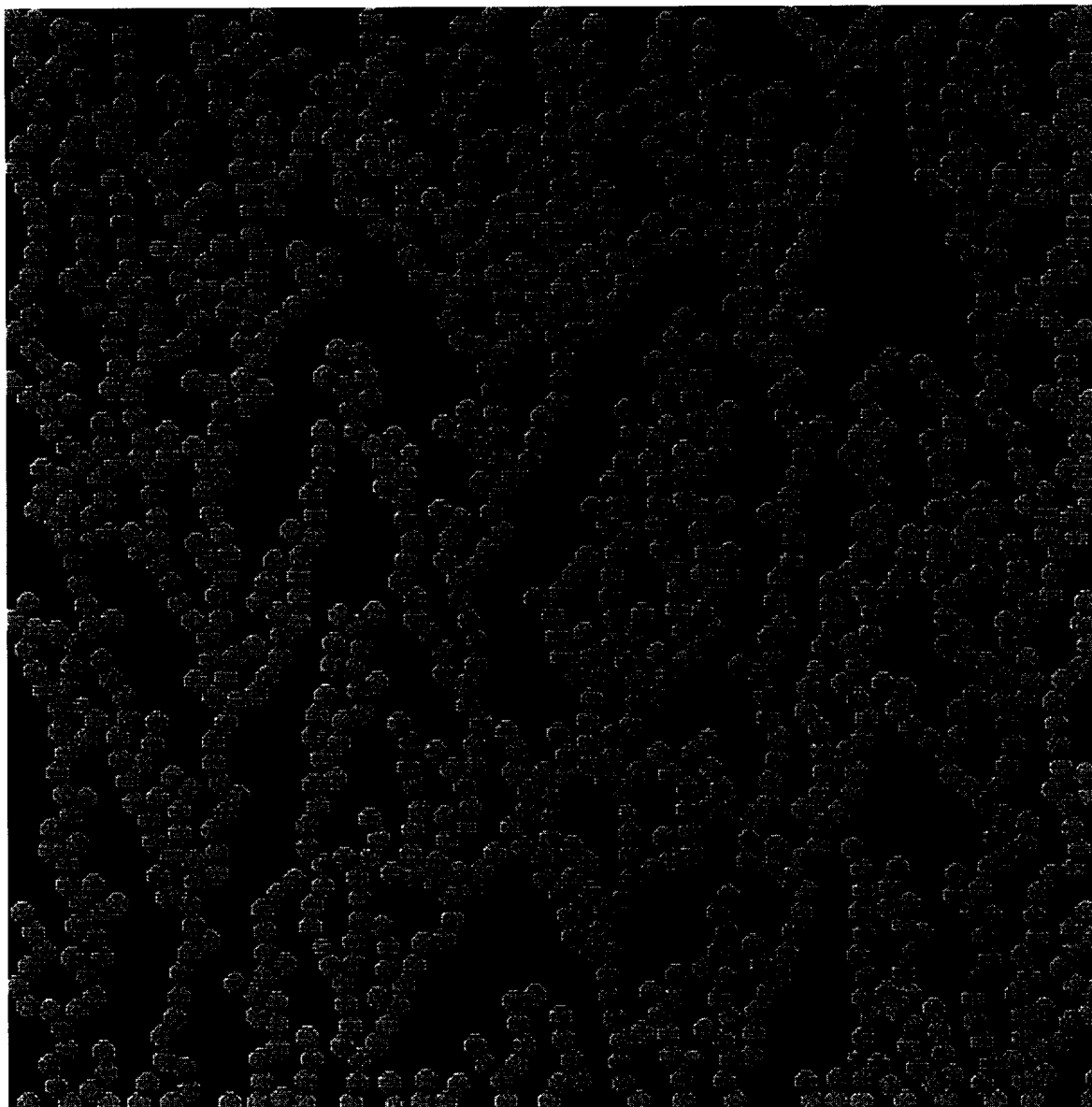


Fig. 2. Example of 2D random packing of spheres, with unit sticking probability.

media is the determining factor for flux decline and the process is called *surface filtration*. Cake formation may be conveniently simulated using the sphere packing model. For a given thickness of the cake, its resistance to the permeate flow may be computed via the random network model, or simply estimated using the *Carman–Kozeny relation*. If, on the other hand, $\alpha \ll 1$ (i.e. particles are much smaller than the pores), particles can penetrate into the porous media, causing the *internal*

fouling of the membrane. In this case, the particles may be captured inside the porous media through either *particle deposition*, or pore *blinding* and *blocking*, or a combination of these mechanisms. Here a particle trajectory analysis, similar to that used by Imdakm and Sahimi [9], may be employed to predict the fate the penetrating particles. In between the two extrema (i.e. $\alpha \sim 1$) is the case where both cake formation and internal fouling are equally important. To simulate this sit-

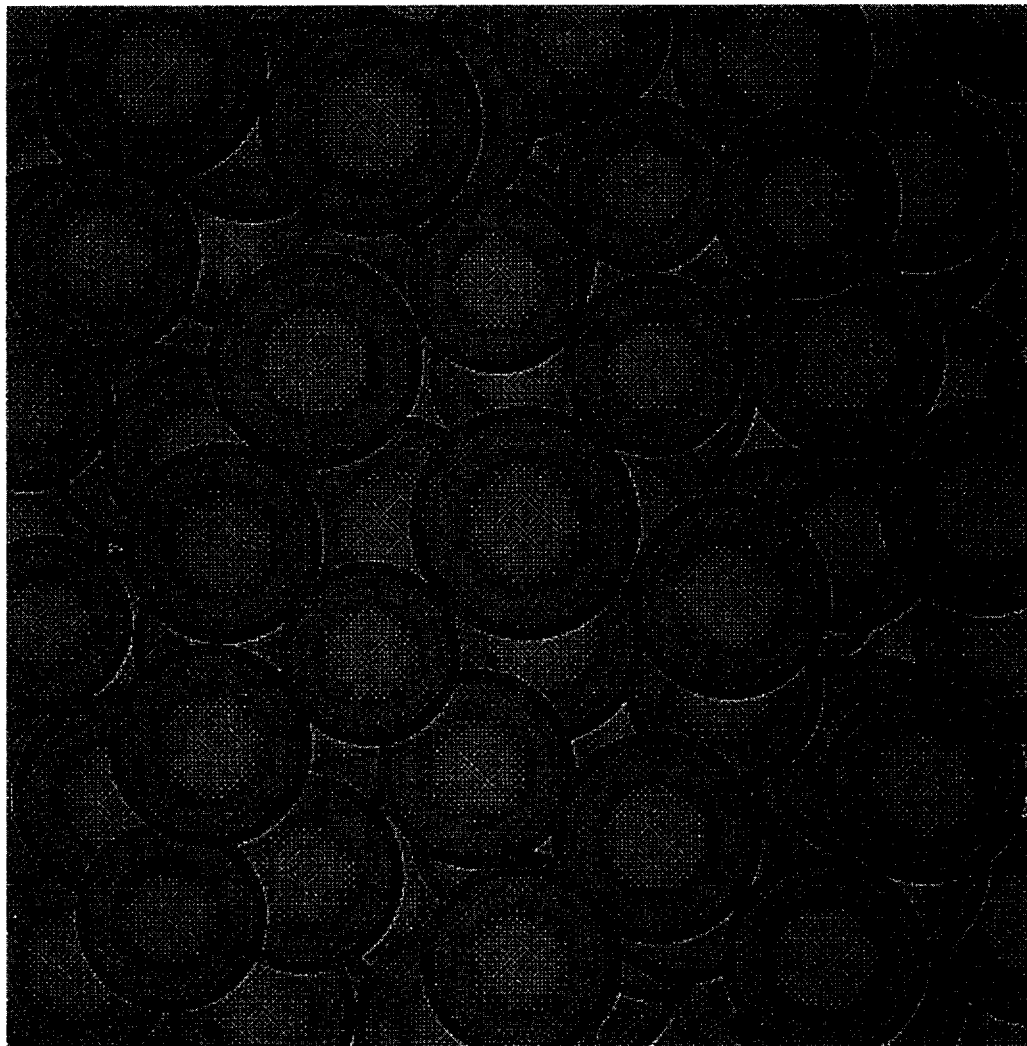


Fig. 3. Example of 3D random packing of spheres, with zero sticking probability.

uation, a combination of the two basic models may be used.

The simulation model can be applied to both *dead-end* filtration and *cross-flow* filtration modes, and as far as the simulation model is concerned, the only difference between the two is that in the latter mode not all the particles reaching the surface of the porous media can be retained by the porous media. To determine whether a particle reaching the membrane surface can actually be held on the membrane surface, a torque-balance analysis first proposed by Lu and Ju [10] and more recently generalised by Stamatakis and Tien [11], may be employed.

Details of the two basic models are given below. The procedures for applying the models to the membrane filtration processes, together with necessary improvements and modifications, will be illustrated through some case studies.

2. Model description

2.1. Sphere packing model

To generate the model structure of unconsolidated, or slightly consolidated, granular porous media, a sim-

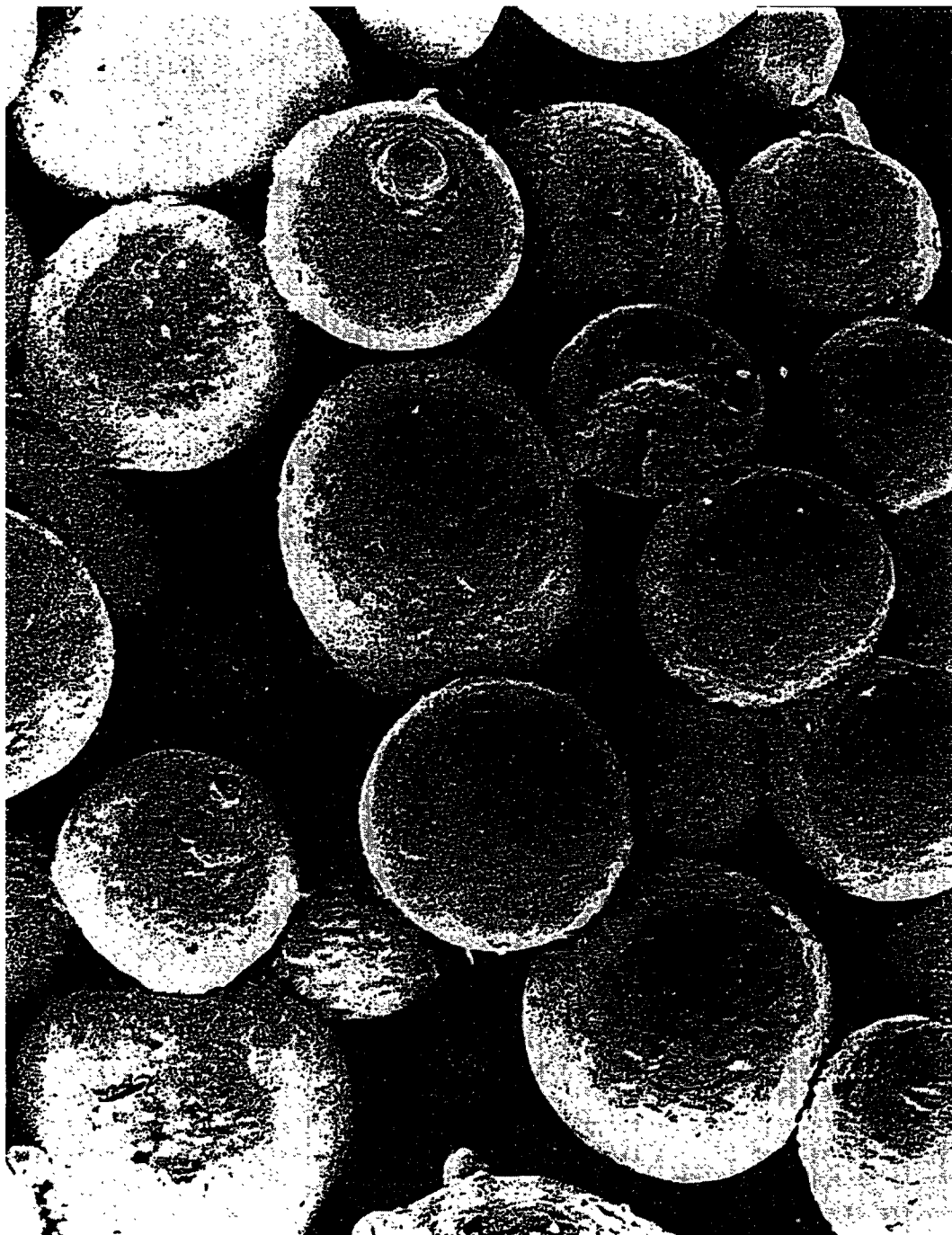


Fig. 4. Photomicrograph of a sintered metal membrane.

ulation model based on the algorithm of Vold [2] can be used. Details of this ballistic sphere-settling algorithm have been given by Vold [2], but a brief account of the model is given below.

The model considers the stable configuration of a distribution of spheres in a containment volume. A Lagrangian description is used to form a random packing by adding one sphere at a time to the assembly. The

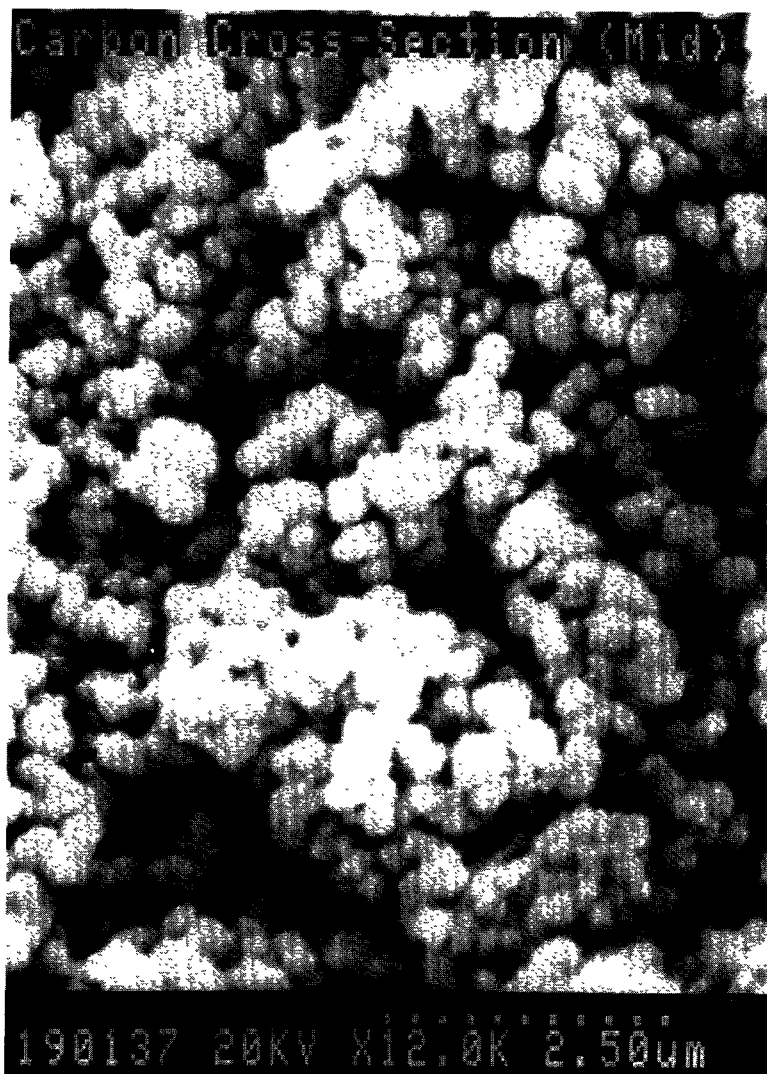


Fig. 5. Photomicrograph of a sintered carbon membrane.

assembly is formed by dropping a sphere from a random entry position in a fixed plane above the containment volume. The simulation starts with the containment volume empty. When the first sphere is added it reaches the bottom or base plane of the volume and remains at the position of contact. The process is repeated adding one sphere at a time, an assembly builds up. The rules for determining the equilibrium position of each sphere are carefully defined. If a sphere reaches the base plane it remains in the arrival position. If a sphere lands on a stack of spheres two conditions are tested. If the sphere is similar in size to those at the arrival position then it is allowed to roll over the surface

of the contact sphere(s) until it reaches a stable location. It is possible to alter the fate of the settling sphere, hence the structure of the packing, by introducing a so-called *sticking probability*. Upon each contact the settling sphere makes with others a probability test is performed against this sticking probability to decide whether it will continue to roll or will “stick” to the sphere it has just contacted. If the particle is small in relation to the surrounding particles in the packing, then it may navigate through the pores in between the packed spheres. The model assumes that the actual path followed by the settling sphere can be represented as a series of geometrical trajectories, a straight line when

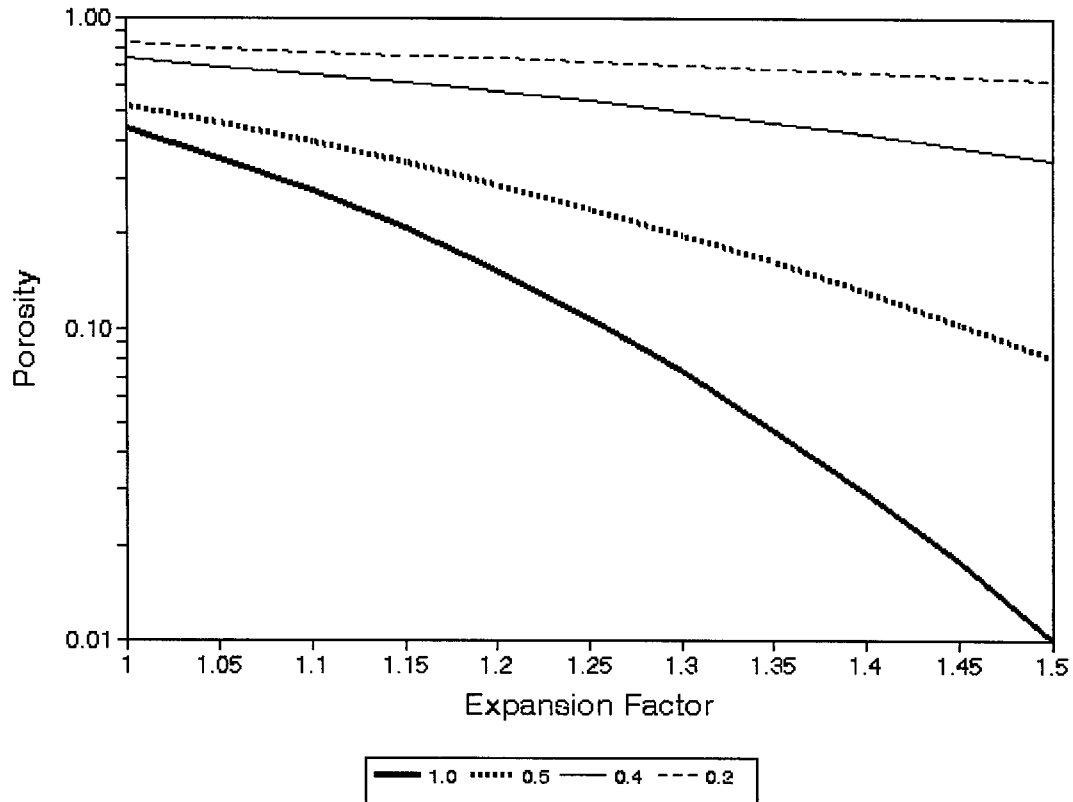


Fig. 6. Dependence of the porosity on the expansion factor and primary/cluster size ratio.

the sphere is free falling, or part of a circle when it is rolling over the surface of other spheres.

Vold's algorithm has been chosen mainly for its versatility and efficiency. Its efficiency stems from the algorithm's deterministic nature. Its versatility may be seen from the following remarks. First, the algorithm can easily be adapted to utilise various boundary conditions. In our simulation, the absorbing virtual walls used in Vold's original algorithm are replaced by the *periodical boundary conditions*, in order to eliminate the edge effect. Secondly, the use of the sticking probability makes it easy to control the structural properties (e.g. porosity) of the sphere packing. Variation of the porosity with the sticking probability for different mean standard deviation/mean size ratios (assuming normal size distribution) is shown in Fig. 1. And thirdly, the algorithm can be applied to both 2D and 3D space without any procedural changes.

Fig. 2 shows an example of the 2D structure generated using the modified algorithm. The sticking probability in this case is set to be 1, which implies that

during the simulation a sphere will stick and stay in place upon the first contact with others. The fractal-like structure resembles that of the dust deposits on fibres often found in air filtration. Fig. 3 shows a 3D packing generated with the sticking probability being 0, i.e. all spheres are in a mechanically stable position. The structure is similar to that of a sintered metal membrane shown in Fig. 4.

For some sintered granular membranes, the globules distinguishable under low or medium resolutions are actually made up of smaller (or primary) particles which can only be seen at high magnifications. Further, there are severe overlaps at both the primary and the secondary levels. An example of such membranes is given in Fig. 5, where the mean diameter of the globules is about $0.5 \mu\text{m}$ and the mean diameter of the primary particles is about $0.18 \mu\text{m}$.

This kind of consolidated structure can be simulated by modifying the basic model structure as follows. First, increase the size of each packed sphere slightly, without changing their position, to create partial over-

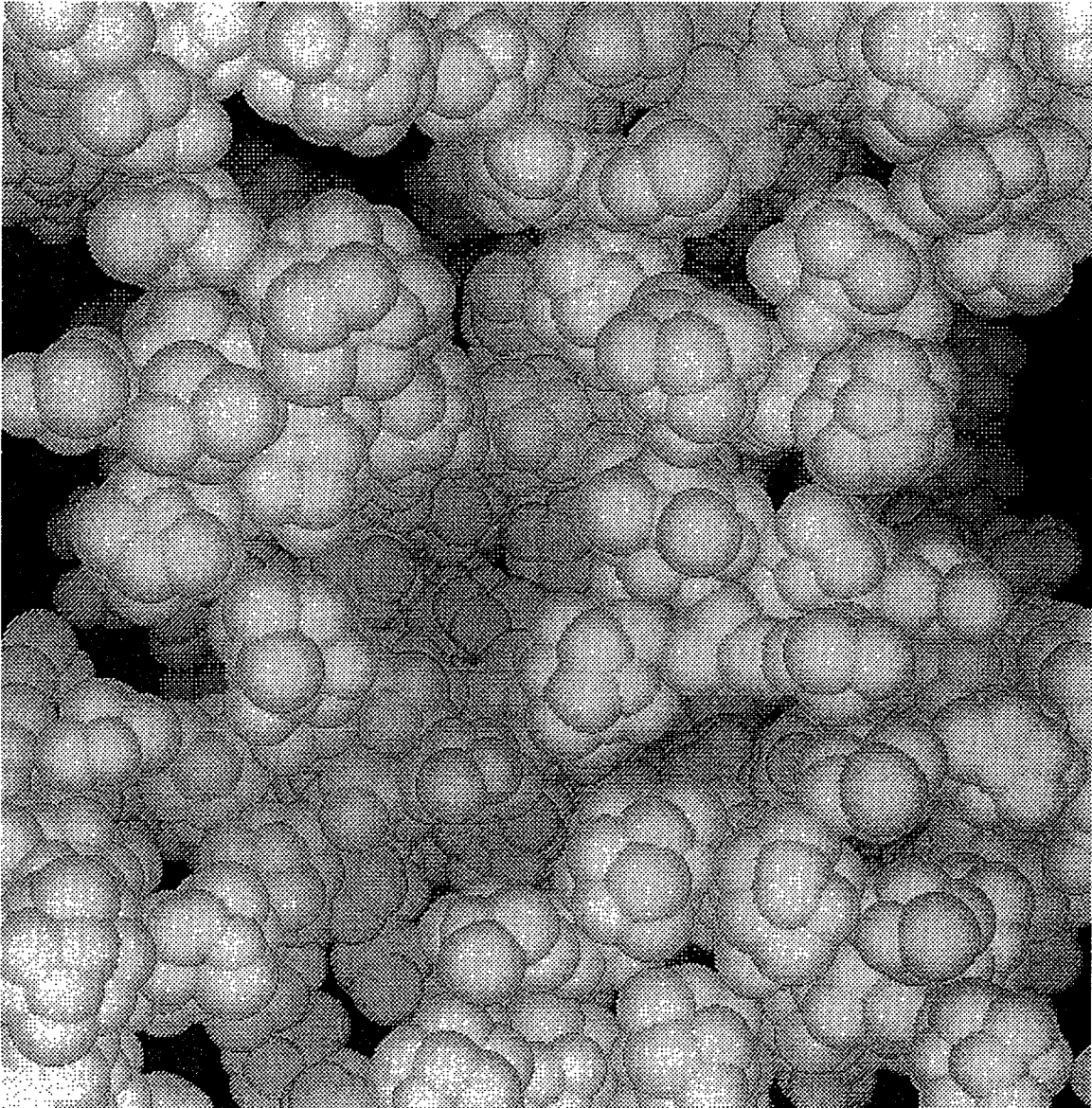


Fig. 7. Simulated structure of the sintered carbon membrane.

laps between the spheres. Then, replace each enlarged sphere with a spherical floc of roughly the same size as the enlarged sphere but consisting of smaller spheres. Finally, if necessary, increase the size of the primary spheres to create partial overlaps between the primary particles within each floc. The consolidation has a profound effect on the porosity of the resulting structure. The porosity is also dependent on the relative size of the primary particles, but to a lesser extent. This can be seen from Fig. 6.

Fig. 7 is an example of the resulting structure, which compares well with the actual membrane shown in Fig. 5. It was constructed from an original packing of 914 spheres with 0.5 mm mean diameter and 0.1 mm standard deviation. The original packing was first consolidated with an expansion factor of 1.25, then the spheres were replaced by clusters consisting of 26485 primary spheres of 0.18 mm mean diameter and 0.05 mm standard deviation. Finally, the packing was consolidated again using an expansion factor of 1.50.

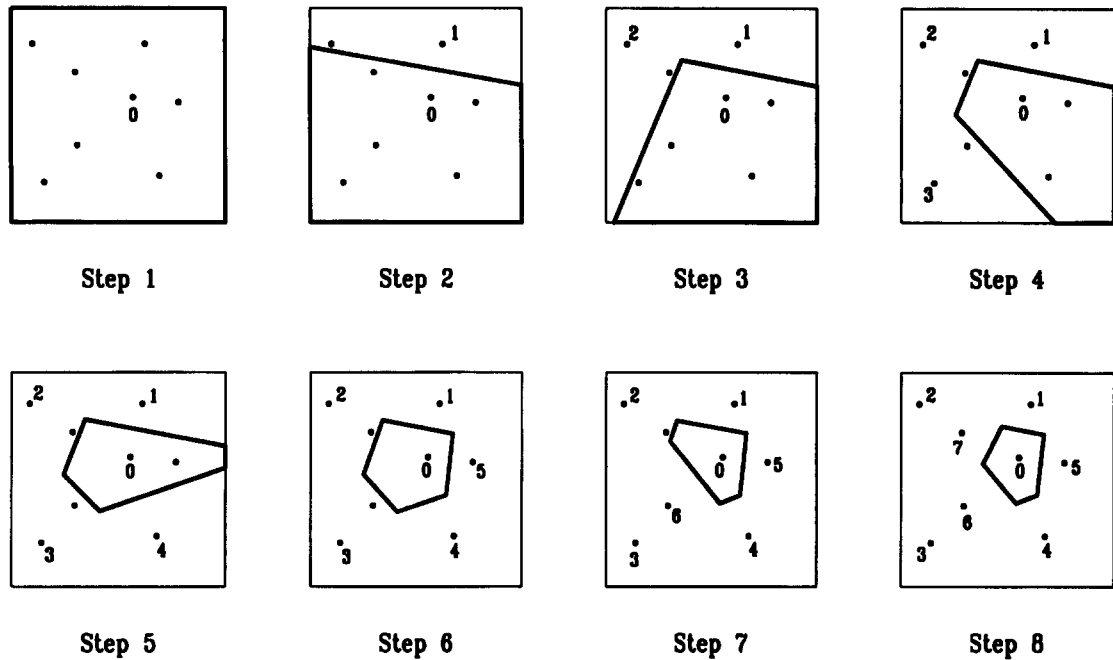


Fig. 8. Schematic diagram showing the procedure of box-chopping algorithm.

2.2. Random network model

If the space occupied by a random packing of equal spheres is divided using the *Voronoi tessellation*, with the centres of spheres being the seeds, then each Voronoi cell contains a unique sphere, each vertex in the tessellation lies in the middle of a unique pore body, and each of the cell edges passes through a unique pore throat. These properties suggest that, for a packing of equal spheres, the Voronoi tessellation may be used as the skeleton upon which a random network of, for example, cylindrical tubes can be constructed to represent the interconnected pores in the porous medium. The axes of the tubes coincide with, or parallel to, the edges. The lengths of the tubes are equal to the lengths of the corresponding edges. The radius of each tube is calculated based on the average distance from the tube axis to each of the surrounding spheres. Since the tube is not an exact representation of the actual pore geometry, the radius of each tube is less well-defined and the exact value depends on which property the model is meant to preserve. For instance, to maintain the porosity of the packing, it should be adjusted so that the sum of the tube volume equals the total free volume of the packing. As far as pore blockage/blinding is con-

cerned, the tube radius should be given a value corresponding to the narrowest part of the pore.

If the packing consists of unequal spheres, the Voronoi tessellation is no longer applicable because some of the edges, hence the tubes built on them, will cut through the packed spheres. In order to tessellate the packing of randomly-sized spheres, a general tessellation algorithm has been devised, which uses the following intersecting plane to draw the boundary between two spheres denoted by (x_i, y_i, z_i, a_i) and (x_j, y_j, z_j, a_j) , respectively:

$$(x_i - x_j)X + (y_i - y_j)Y + (z_i - z_j)Z = \frac{1}{2}[(x_i^2 + y_i^2 + z_i^2 - a_i^2) - (x_j^2 + y_j^2 + z_j^2 - a_j^2)] \quad (1)$$

The tessellation obtained in this manner has the following useful properties. First, for a given set of spheres, the tessellation is uniquely defined. Each cell surrounds a unique sphere, and the edges pass through the pores and do not penetrate the spheres. Secondly, if the spheres are of the same size, the Voronoi tessellation is obtained. Thirdly, it can be used for both 2D and 3D packings, with no restrictions on the packing density,

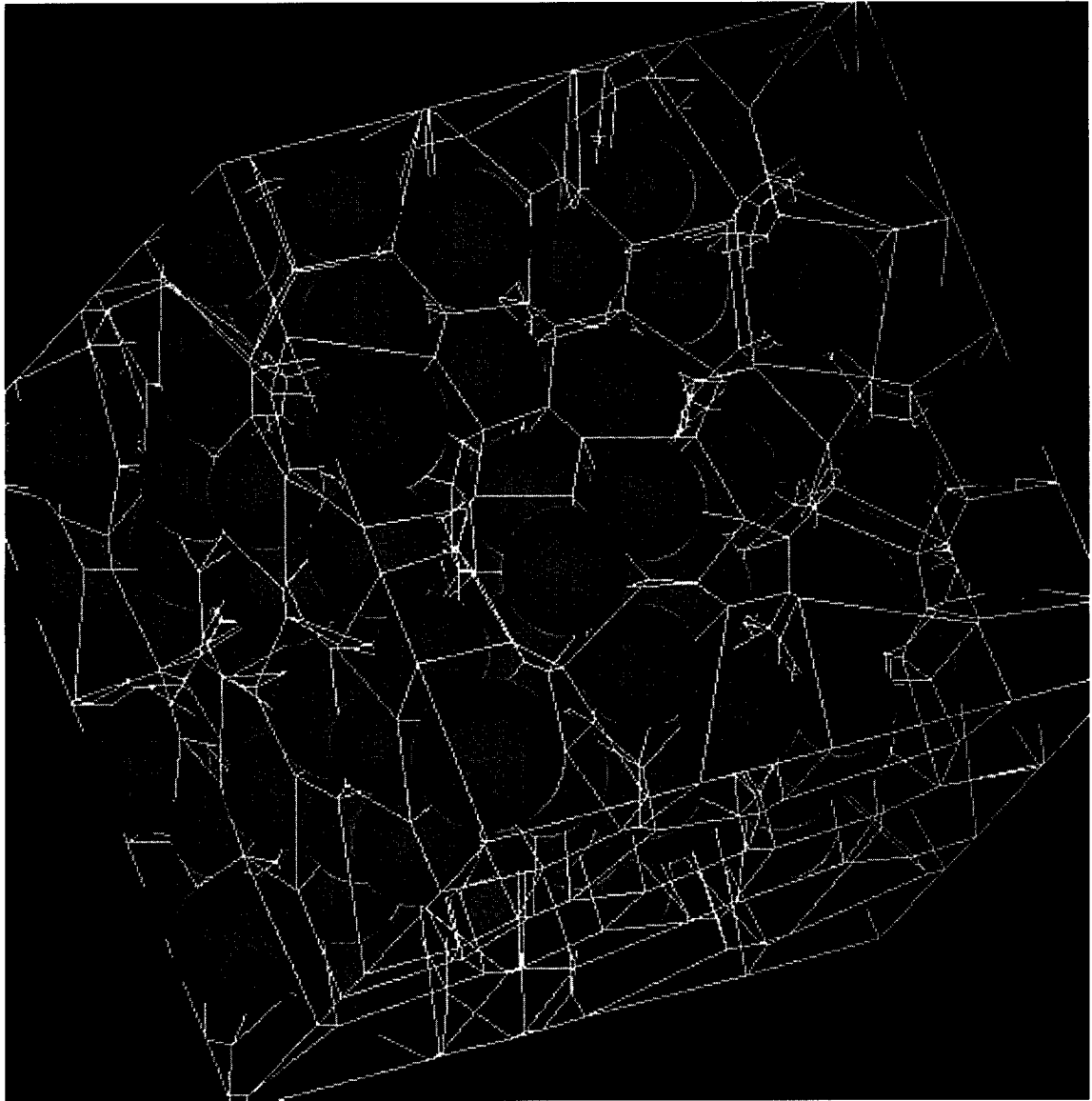


Fig. 9. Example of the skeleton of the generated random network.

whether the spheres overlap with each other, or whether the spheres are randomly packed or orderly arranged. Analogous to the physical interpretation of Voronoi tessellation, this tessellation corresponds to a growth process in which the growth rate is different for each of the spheres and is size-related.

Most algorithms available for the Voronoi tessellation cannot readily be adapted for use with this general scheme, because those algorithms rely heavily on some geometrical properties peculiar to the Voronoi tessel-

lation. To implement this general tessellation scheme, a box-chopping algorithm has been used. To construct a cell surrounding a given sphere, an initial cubic box, centred at the given sphere and large enough to contain all the spheres close to the given sphere, is chopped step by step into the final shape, using the intersecting planes defined by Eq. (1). The procedure is depicted in Fig. 8, and a tessellation of a random packing of unequal spheres generated using this general algorithm is shown in Fig. 9.

There are many interesting properties of the random network that can be calculated by the simulation program, of which the most relevant include the distributions of tube length and tube radius in relation to packing characteristics because these directly affect flow distribution and particle capture efficiency of the simulated porous media.

In general, the average tube length is roughly the same as the mean sphere radius, and the tube radius is about half the mean sphere radius. For example, the random network generated based on a close random packing of 911 spheres, with 1.0 mean radius and 0.1 standard deviation and 0.51 overall porosity, consists of 10822 tubes:

Tube radius: Min \approx 0.0, Max = 2.54, Mean = 0.51

Tube length: Min \approx 0.0, Max = 5.79, Mean = 1.00

Fig. 10 shows the distribution of tube length and radius. It can be seen that most tubes have a size close to its lower limit, and the distributions may be better

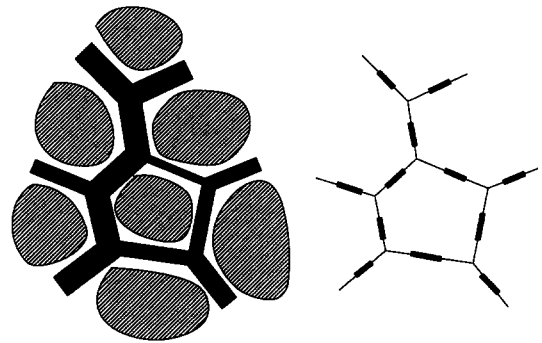


Fig. 11. Analogy between fluid flow network and electrical current circuit.

described by a log-normal than by a normal distribution function.

It is well recognised that the topology as well as geometry of a network affects the fluid distribution in, and hence predictions of filter performance made from, the network. A key parameter describing the topology

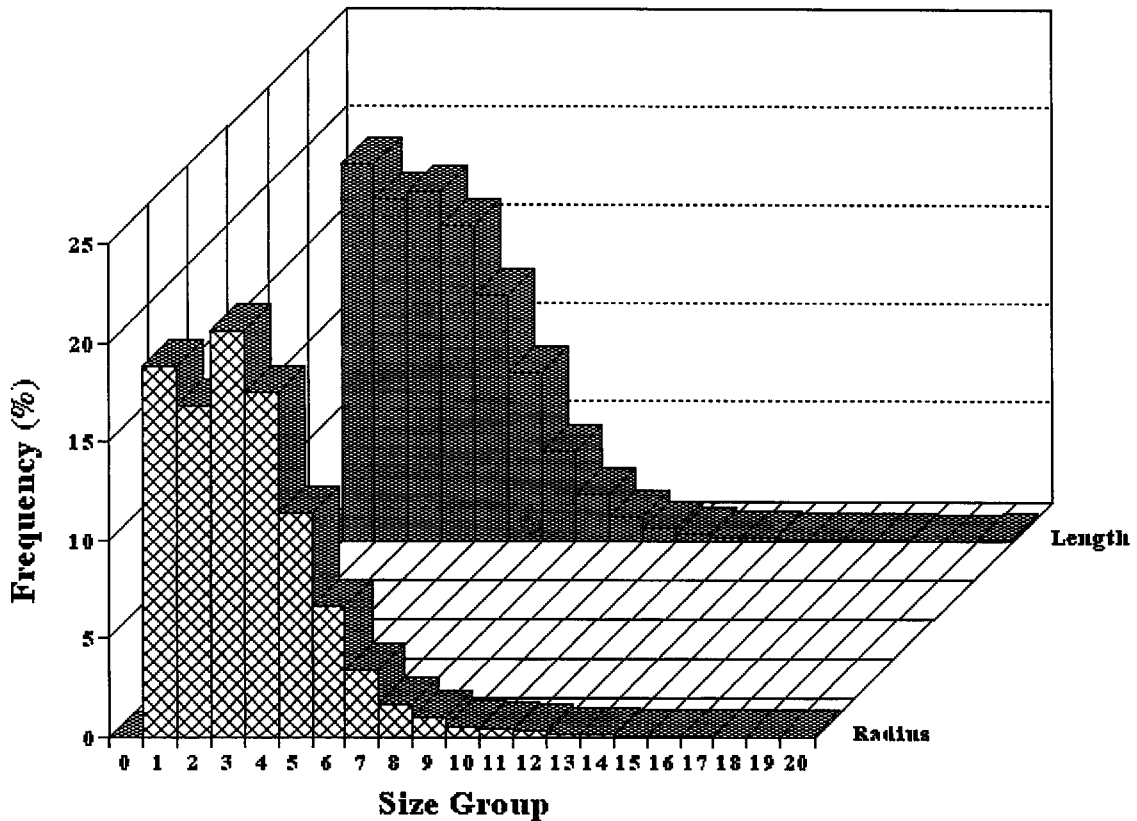


Fig. 10. Distribution of tube length and radius.

of a network is the average coordination number, i.e. the number of pores joined at each node in the network. In a randomly packed granular medium such as sandbed, the average coordination number is most likely to be 4, as indicated by results from the tessellation of random packing of spheres, rather than 6, as in a regular cubic lattice network. In this respect, a square lattice network, which has an average coordination number of 4, is topologically a better representation of the granular porous media, and is simpler since it is a 2D model.

3. Model applications

3.1. Flow distribution in porous media

In a porous medium such as a sintered carbon membrane filter, each pore accessible to the flow exhibits a hydrodynamic resistance, together the interconnected pores form a resistive network. The whole network behaves like a single resistor to the flow. Therefore, to find the total flow rate for a given pressure drop across the network or vice versa, all we need to know is the total resistance of the network. Although the total hydrodynamic resistance of a given porous medium may be measured experimentally or estimated using some simple semi-empirical relation such as the Carman–Kozeny equation, neither can give details of flow distribution within the porous medium, and yet

Table 1

Summary of conditions and results of flow distribution calculation

Parameter	Value	Units
Mean sphere radius	0.25	μm
Standard deviation	0.025	μm
Length of simulation box	5	μm
Number of spheres	975	
Packing porosity	0.438	
Number of nodes	6961	
Number of tubes	13674	
Mean radius of tube	0.0857	μm
Mean length of tubes	0.2204	μm
Pressure drop	418.7	Pa
Superficial velocity	8.0	$\mu\text{m}/\text{s}$

such details are essential for a better understanding, design and control of the filtration process or equipment.

With the random network model, it is possible to calculate the flow distribution inside porous media, provided the resistance of each individual pore is known. In our simulation, each individual pores is represented by a cylindrical tube and the flow through the tube is assumed to be laminar so that the relation between the pressure drop Δp and volume flowrate Q can be expressed by Hagen–Poiseuille equation:

$$Q = \left[\frac{\pi r^4}{8 \mu l} \right] \Delta p \quad (2)$$

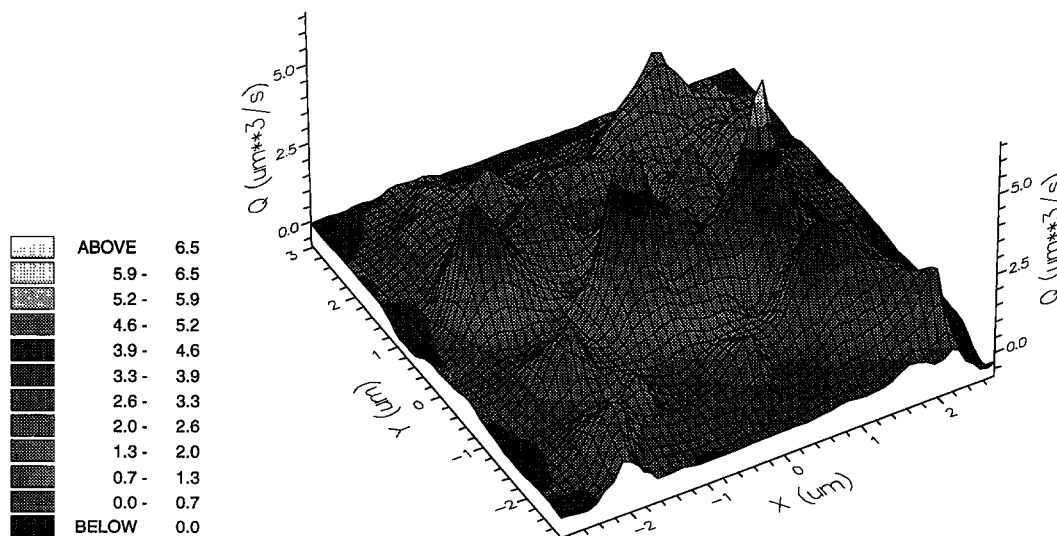


Fig. 12. Flow distribution in a cross-sectional plane.

where a_p denotes the tube radius, l its length, and μ fluid viscosity. This relation states that the volume flowrate is linearly proportional to the pressure drop, and the hydrodynamic resistance R depends only on the properties of the fluid and the tube:

$$R = \frac{8\mu l}{\pi r^4} \quad (3)$$

Given the resistance of individual pores, the fluid flow through the network can be calculated by analogy with the current through an electrical network, as illustrated in Fig. 11.

Two methods may be used to calculate the network flow. One is the so-called loop approach, in which the total resistance is calculated by solving a set of equations written for each of the individual nodes and distinctive loops in the network, according to Kirchhoff's current and voltage laws, respectively. The total number of equations to be written and solved is equal to the total number of tubes in the network. Although conceptually straightforward, it is only suitable for sim-

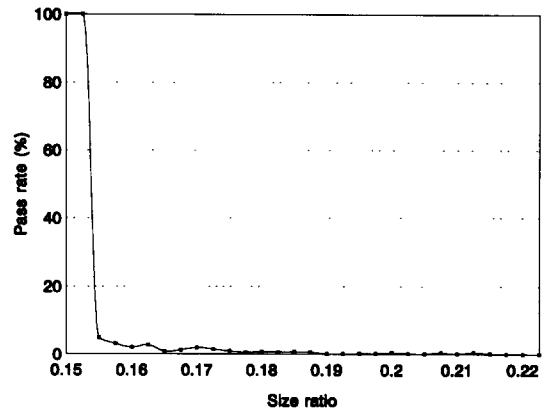


Fig. 14. Pass rate as a function of size ratio for packing of equal spheres.

ple networks because it entails identification of all uncorrelated loops or removal of all redundant loops in the network, which is a very tedious and error prone task. For large and complex networks, it is more convenient to employ the so-called *nodal approach*. This approach only requires that a nodal pressure equation be written for each of the nodes in the network:

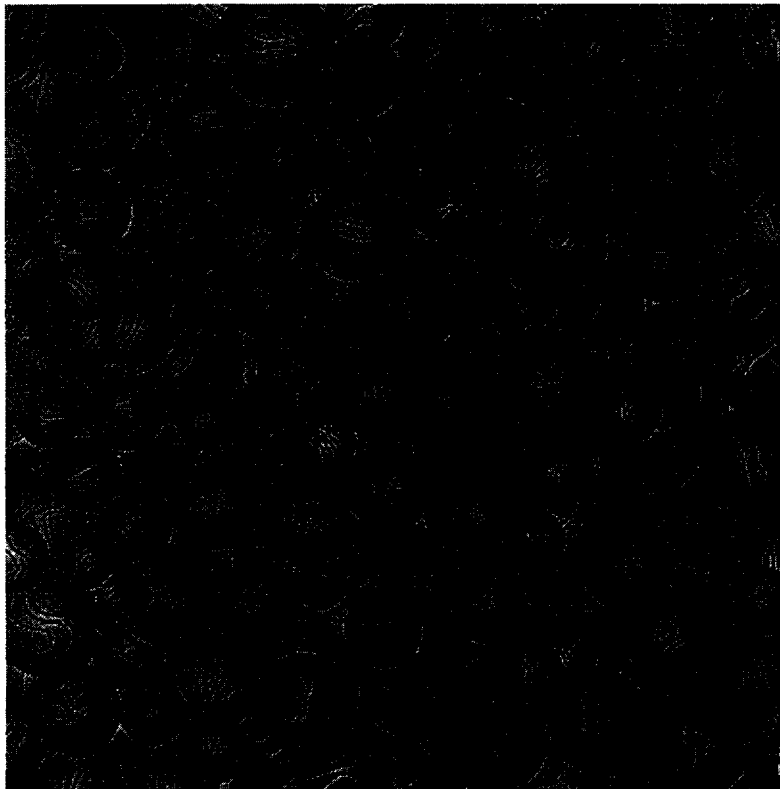


Fig. 13. The match between cross-sectional flow distribution and the packing image.

Table 2
Comparison between random network model and Carman–Kozeny equation

Packing dimension	Number of spheres	Ratio of difference	Packing dimension	Number of spheres	Ratio of difference
6.0	22	3.96688	6.5	29	3.74984
7.0	35	2.96102	7.5	45	3.21356
8.0	58	4.03328	8.5	68	4.63097
9.0	83	3.13694	9.5	99	3.34843
10.0	115	4.15248	10.5	136	3.45916
11.0	158	3.34140	11.5	185	3.22293
12.0	206	3.75335	12.5	236	3.81197
13.0	264	3.5062	13.5	291	3.76426
14.0	331	3.76518	14.5	370	3.81148
15.0	412	3.56317	15.5	454	3.92081
16.0	499	3.74674	16.5	547	3.96570
17.0	613	3.75659	17.5	666	4.14895
18.0	722	3.71770	18.5	790	3.89466
19.0	857	3.63468	19.5	919	3.80523
20.0	1000	4.20413	20.5	1078	3.74213

$$\sum g_{ij} \Delta p_i = 0 \quad (4)$$

Here g_{ij} is the hydraulic conductance, equal to the reciprocal of the resistance, of tube j connected to node i ; and p_i is the nodal pressure. Since in our random network model the number of nodes is only about half the number of tubes, the nodal approach is much more efficient in computational terms.

Once the nodal pressure distribution is obtained, the flow distribution and the total resistance of the network, can be calculated. Fig. 12 shows the flow distribution in a horizontal cross-sectional plane of a random packing of spheres; conditions and results are summarised in Table 1. Fig. 13 presents the same data but in a different style in order to show the correlation between the flow pattern and the packing structure.

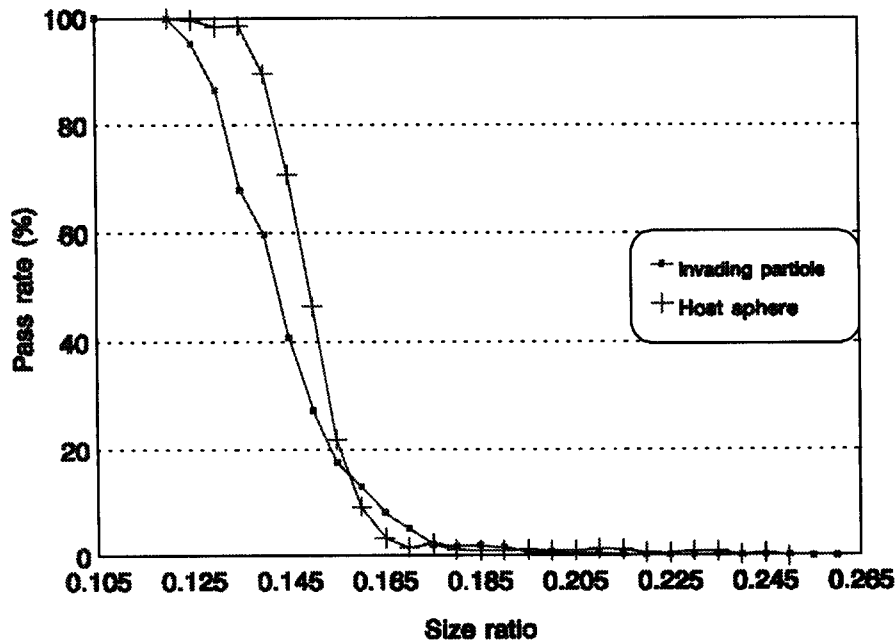


Fig. 15. Pass rate as a function of size ratio for packing of unequal spheres or randomly sized invading particles.

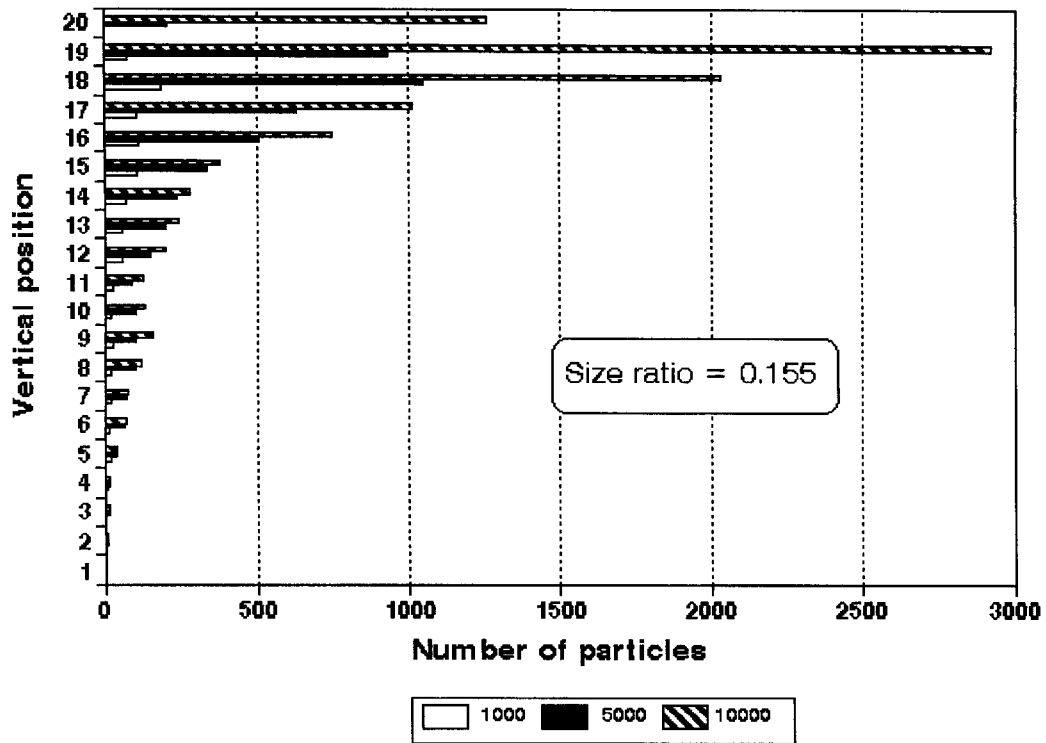


Fig. 16. Particle number concentration distribution in a host packing of equal spheres.

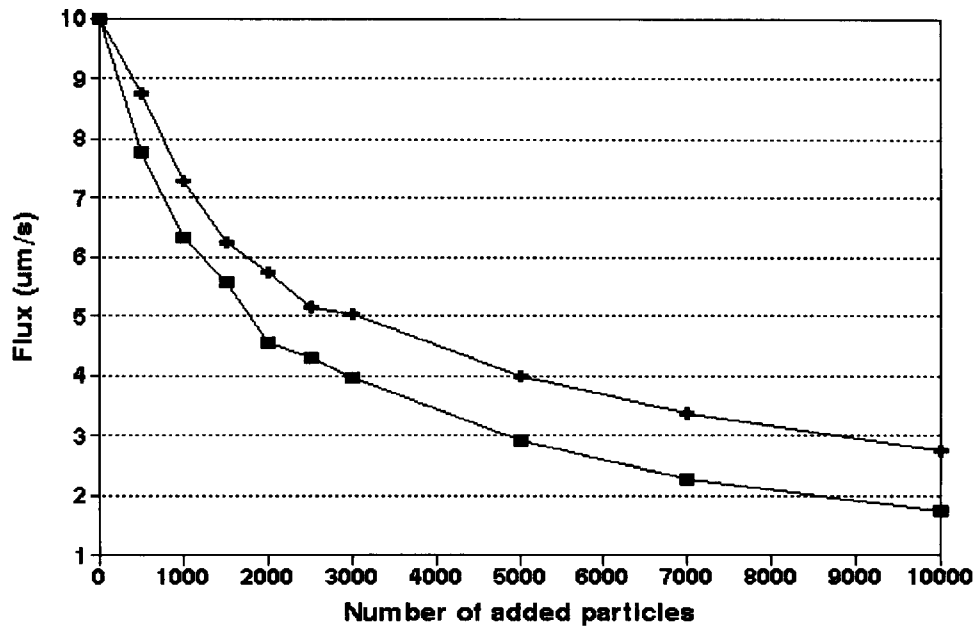


Fig. 17. Flux decline with equivalent time for different particle sizes.

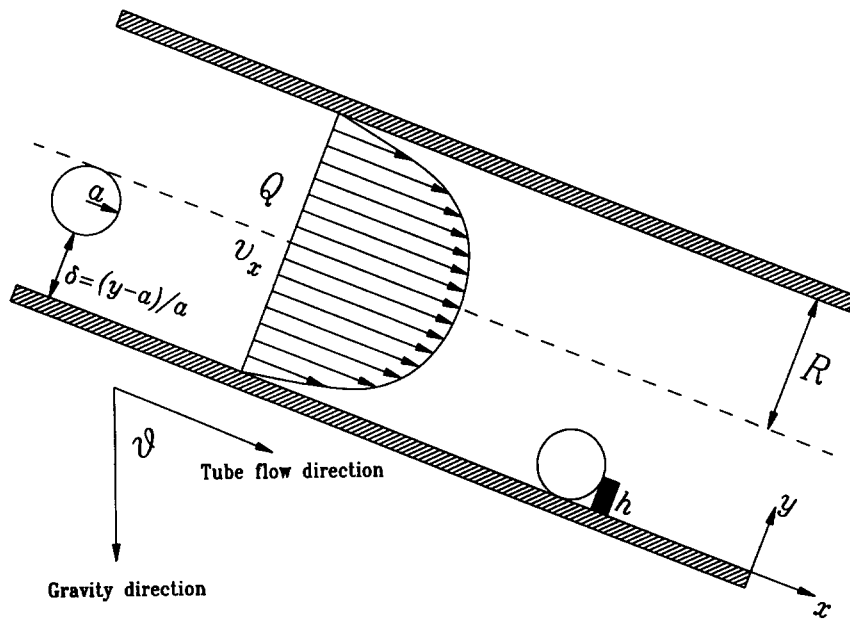


Fig. 18. Schematic representation of particle transport and deposition in a tube.

Carman–Kozeny relation is a well-established semi-empirical equation to calculate the pressure drop Δp required for a fluid of viscosity μ to flow at superficial velocity U_s through the depth L of a packing of porosity ϵ , consisting of identical spheres of diameter d :

$$\Delta p = \frac{180\mu(1-\epsilon)^2 L U_s}{\epsilon^3 d^2} \quad (5)$$

To validate the random network model, model predictions have been compared with Carman–Kozeny estimations for a number of cases. This is summarised in Table 2 below. In all calculations listed in the table, the mean radius of spheres was 1.0 arbitrary units. The simulation box is cubic, whose sides are measured in the same units, and termed packing dimension in Table 2. It can be seen from Table 2 that, in most cases, the model predictions differ from the Carman–Kozeny estimations by an almost constant factor between 3 and 4. Thus, in practical applications of the model, a correction factor of 3.7243, obtained by averaging the ratio of differences listed in Table 2, may be used.

3.2. Internal membrane fouling

When $\alpha \ll 1$, particles can penetrate into the porous media, causing internal membrane fouling. Possible

mechanisms for particle trapping include pore blocking or blinding and particle deposition.

Simulation using sphere packing model

If the focus of the simulation is on the mechanical, as opposed to chemical, trapping of the particles (via pore blocking or blinding), the sphere packing model may be used. The procedure is to first generate the host medium, then add small particles using the same algorithm. Since no physicochemical interactions are involved in the simulation, the absolute or real size of the particles is irrelevant. It is more convenient to use size ratio, α , here. Fig. 14 shows the predicted relation between the size ratio and the pass rate (defined as the ratio of the number of particles passing through the medium to the total number of particles added during the simulation). In this simulation, both the host grains and the suspended particles are uniform sized spheres. The sudden drop in the pass rate at size ratio between 0.1525 and 0.1550 suggests that, for porous media of equal sized spheres, there exist a critical size ratio, above which almost all particles can be retained by the media but below which almost particles can pass through the media. Once the size ratio passes the critical value, the pass rate declines gradually and becomes virtually zero at about 0.2175. This indicates that the

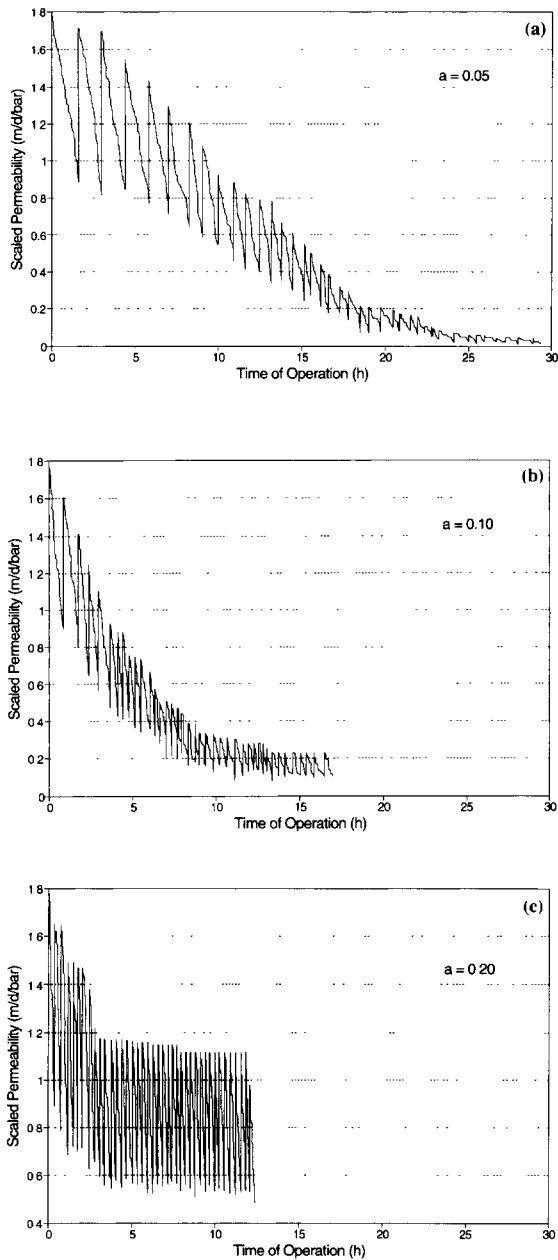


Fig. 19. Flux decline for (a) $a = 0.05 \mu\text{m}$, (b) $a = 0.1 \mu\text{m}$ and (c) $a = 0.2 \mu\text{m}$.

pore throats in the porous media have a fairly narrow size distribution, ranging from 0.1550 to 0.2175.

If the host medium consists of spheres of randomly sized spheres, the pore sizes will have a wider distribution. In addition, the sudden drop in the pass rate has

now become a gradual decay. This can be seen in Fig. 15, where spheres forming the host medium have a 10% standard deviation in size, but the invading particles are equal-sized. If the invading particles are randomly sized, similar effect can be observed. This is also shown in Fig. 15, where the particles have a 10% standard size deviation but the host spheres are equal-sized.

During the initial stage of filtration when all the pores are accessible, the invading particles have an equal opportunity over the entire depth of the porous medium of being trapped. Thus the initial penetration is fairly uniform. Once particles start to clog the pores, at the top of the porous medium, there is a reinforcing effect

Table 3
Conditions used in simulations of filtration/backflushing

Parameter	Value	Unit
Mean radius of host spheres	0.25	μm
Standard size deviation	10%	μm
Porosity of host medium	0.45	
Mean tube radius	0.09	μm
Mean tube length	0.25	μm
Surface roughness	25	nm
Mean radii of invading particles	0.05, 0.1, 0.2	μm
Standard size deviation	20	%
Particle mass density	1.5×10^3	kg m^{-3}
Particle zeta potential	-6	mV
Pore surface potential	25	mV
Ionic strength	1	mol dm^{-3}
Effective Hamaker constant	1×10^{-20}	J
Filtration pressure differential	1.25×10^8	Pa m^{-1}
Backflushing pressure differential	1.25×10^8	Pa m^{-1}

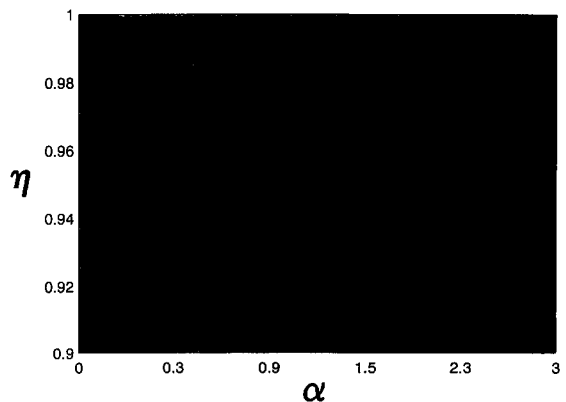


Fig. 20. Backflushing efficiency as a function of the size ratio.

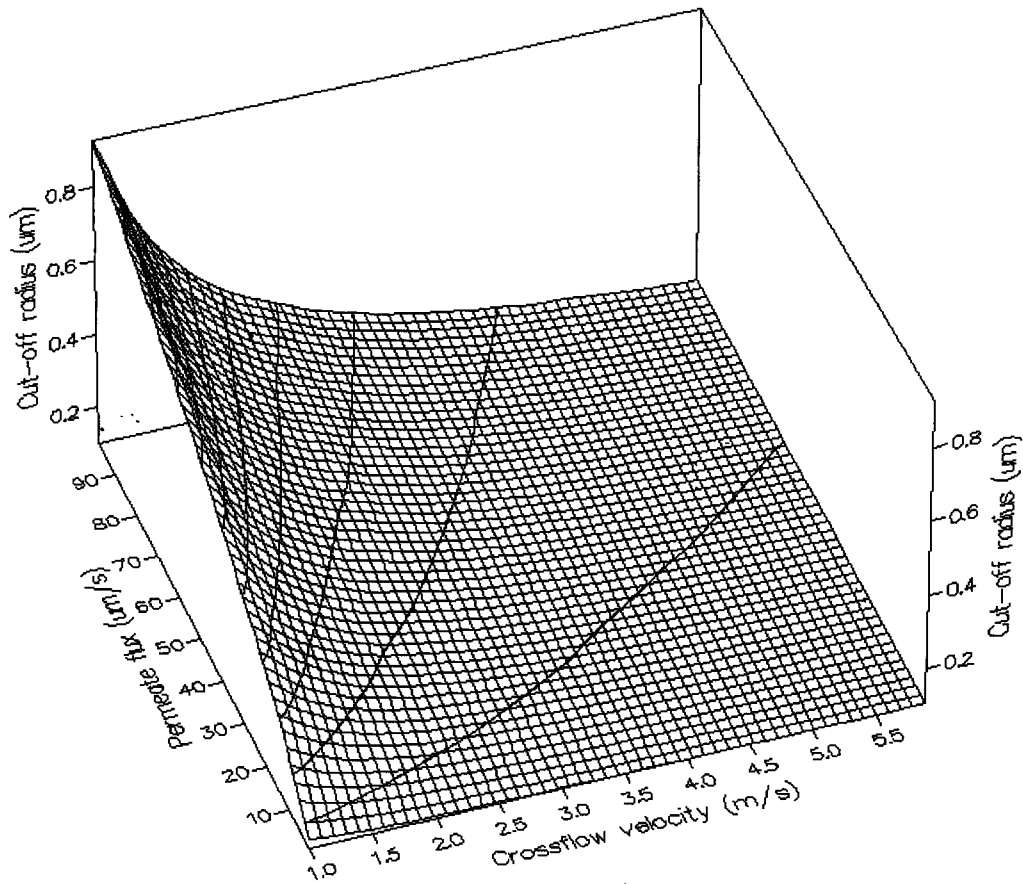


Fig. 21. Cut-off radius as a function of crossflow and permeate flow velocities.

and subsequent invading particles will find it increasingly difficult to penetrate. This results in an excessive accumulation of trapped particles near the top of the porous medium. Eventually, cake starts to build up on top of the porous medium. Particle concentration distribution at these different stages can be seen in Fig. 16.

Using Carman–Kozeny equation, the flux level at different time of particle penetration can be estimated. Examples are given in Fig. 17.

Simulation using random network model

To include the physicochemical adsorption, it is convenient to use the random network representation of the porous medium. A procedure similar to that used by [9] can be employed. It calculates the particle trajectory to determine whether a particle can reach the surface of a pore, and uses a mechanical criterion based on a torque balance to decide whether the particle can

be held on the surface. The trajectory equation is of the following form:

$$\frac{dy}{dx} = \frac{N_G \sin \Theta + N_{E1} (N_{E2} - e^{N_{DL}\delta}) \frac{e^{-N_{DL}\delta}}{1 - e^{-2N_{DL}\delta}} - \frac{N_1 \chi_R}{\delta^2 (2 + \delta)^2}}{4G_1 y R^{-1} + 2G_2 y^2 R^{-2} + G_3 N_G \cos \Theta} \quad (6)$$

Some of the parameters used in the equation are defined graphically in Fig. 18, others have been given elsewhere [9]. The mechanical criterion is:

$$F_y \sqrt{2ah - h^2} \geq 10.205 \pi a^2 \tau_w (a - h) + 3.776 \pi a^3 \tau_w \quad (7)$$

where τ_w is the shear stress at wall.

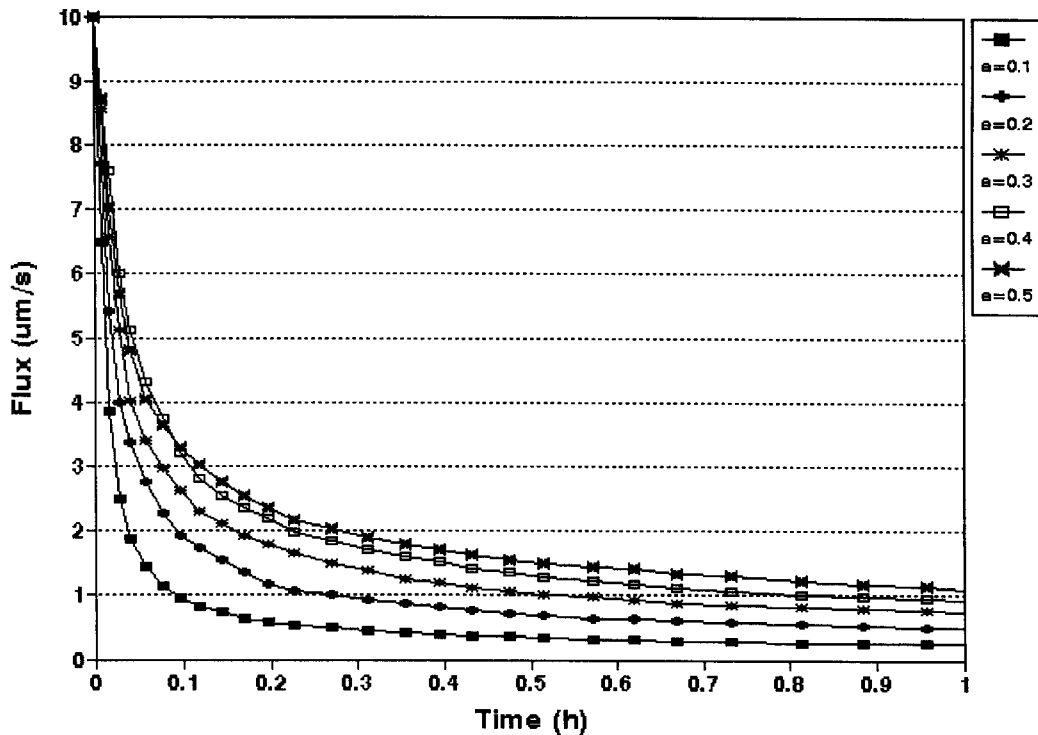


Fig. 22. Flux decline with time for different mean particle sizes.

For particles whose sizes are comparable to the pore sizes, the criteria proposed by Rose and English [12] may be used to decide whether a particle can block or blind a pore:

blocking if $a > 1.1a_p$

blinding if $a_p \leq a \leq 1.1a_p$

Pore blocking is considered to be reversible, because the particle is stopped at the entrance of the pore so that when the flow direction is reversed (during backflushing) the particle can be carried away and the pore entrance reopened. Pore blinding, on the other hand, is regarded as irreversible since the particle is stuck inside the pore and cannot easily be shifted away. This distinction is important when considering backflushing efficiency. Sample results calculated using the above mention procedure are shown in Fig. 19, and corresponding conditions used in the simulation are summarised in Table 3.

In principle, particles retained by surface attraction and/or hydrodynamic forces can be effectively removed through backflushing. However, for particles trapped by geometrical constraints, backflushing effi-

ciency depends strongly on the size ratio, because particles shifted away from their original place may block or blind other pores during backflushing. Fig. 20 shows the backflushing efficiency as a function of the size ratio, obtained using the random network model.

3.3. Cake formation

When $\alpha \gg 1$, particles cannot penetrate into the porous medium but accumulate on top of the medium to form the so-called cake. The cake formation may be simulated using the sphere packing model. If the filtration is operating in the crossflow mode, the torque balance analysis proposed by Lu and Ju [10] and more recently generalised by Stamatakis and Tien [11] may be employed. It uses the following inequality as the criterion to determine whether a particle reaching the membrane surface can stay or be swept away:

$$F_y \sqrt{a^2 - (a-h)^2} \geq F_x (a-h) \quad (8)$$

Solving Eq. (8) gives the cut-off radius a_M :

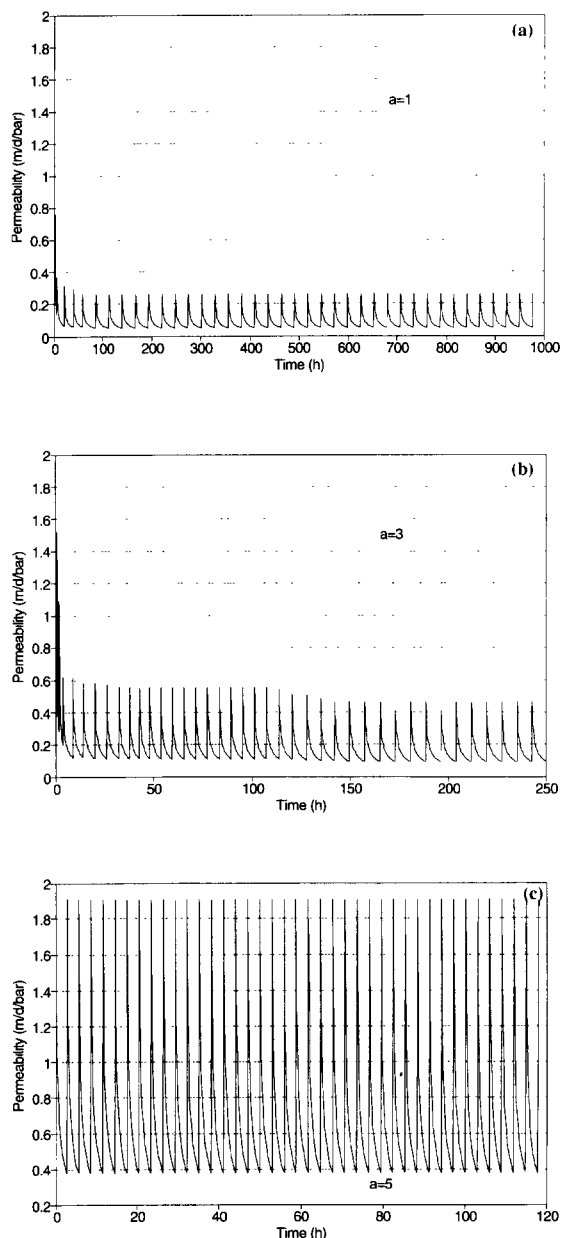


Fig. 23. Permeability vs time at different size ratios: (a) $a = 1 \mu\text{m}$, (b) $a = 3 \mu\text{m}$ and (c) $a = 5 \mu\text{m}$.

$$a_M = \frac{h}{1 - \frac{1}{\sqrt{F_x^2/F_y^2 + 1}}} \quad (9)$$

Fig. 21 shows the variation of the cut-off radius with crossflow and permeate velocities. Other things being

equal, the cut-off radius is directly proportional to the protrusion height, h . Note that the value of the protrusion height is predefined. It is used not only to provide a mechanical barrier for holding particles against the crossflow but also to account for the effects of all the surface interactions which are not explicitly considered in the simulation model. Since it is a lumped parameter, the choice of the value inevitably involves a level of arbitrariness. One of the implications of this uncertainty is that it can sometimes be difficult to compare the simulation results with experimental data quantitatively, even though in principle the model is capable of simulating the essential physics involved in the process of cake formation. Qualitatively, however, the predictions are in good agreement with experimental observations. Fig. 22 shows the flux decline for different mean sizes.

3.4. Simultaneous cake build-up and internal fouling

If the particles are comparable in size with the pores, the external cake build-up and internal membrane fouling will take place simultaneously. To simulate this situation, it may be necessary to combine the two basic models together. For particles smaller than the pores and hence able to penetrate into the porous medium, the random network model is invoked, whereas for those larger than the pores, the sphere packing model is invoked. Fig. 23 shows some examples calculated in this manner.

4. Conclusions

This paper describes a unified approach to simulate filtration/backflushing processes in both dead-end and crossflow modes, on the basis of two simple geometrical models (the sphere packing model and the random network model). We have demonstrated how the random packing of spheres can be used to represent the complex structure of some granular porous media encountered in membrane filtration processes, and how the concept of Voronoi tessellation can be extended to construct a random network which has a morphological link with the model structure and hence is more realistic than existing network models. The simulation model outlined in this paper is self-contained, allowing us to

probe such important problems as how the size distribution of particles constituting the porous media influences the flow distribution, particle capture efficiency and other transport phenomena in the porous media, without resorting to additional assumptions which other network models have to make regarding the correlation between the media and the networks.

5. List of symbols

a	particle radius
a_M	cut-off (or maximum) radius of cake forming particles
a_p	pore size (or tube radius)
d	particle diameter
F_x	net force in the direction of cross flow
F_y	net force in the direction of permeate flow
g_i	hydraulic conductance of tube i
h	protrusion height
l	tube length
L	depth of the packed bed
Δp	pressure drop
p_i	nodal pressure for tube i
Q	volume flow rate
R	hydraulic resistance
U_s	superficial velocity
x_0, y_0, z_0	co-ordinates of cell seed
x_i, y_i, z_i	co-ordinates of surrounding seeds
X, Y, Z	co-ordinates defining the intersecting plane
α	size ratio ($= a/a_p$)
ϵ	porosity

μ	fluid viscosity
τ_w	shear stress at wall

Acknowledgements

The authors wish to thank British Nuclear Fuels PLC for supporting this work.

References

- [1] D.J. Cumberland and R.J. Crawford. *The Packing of Particles*. Elsevier, Amsterdam, 1987.
- [2] M.J. Vold, Computer simulation of floc formation in a colloidal suspension, *J. Colloid Sci.*, 18 (1963) 684–695.
- [3] A.C. Payatakes, C. Tien and R.M. Turian, A new model for granular porous media, *AIChE J.*, 19 (1973) 58–67.
- [4] S.K. Chan and K.M. Ng, Geometrical characteristics of the pores space in a random packing of equal spheres, *Powder Technol.*, 54 (1988) 147–155.
- [5] M.A. Ioannidis and I. Chatzis, Network modelling of pore structure and transport properties of porous media, *Chem. Eng. Sci.*, 48 (1993) 951–972.
- [6] F.A.L. Dullien, Structure of porous media, in J. Bear and M.Y. Coropcioglu (Eds.), *Transport Processes in Porous Media*, Kluwer Academic, Netherlands, 1991, pp. 3–41.
- [7] M.E. Rowley, Flow and Separation of Dispersions in Media Beds and Tilted Plate Separators, Ph.D. Thesis, University of Manchester Institute of Science and Technology, 1988.
- [8] M.P. Hollewand and L.F. Gladden, Modelling of diffusion and reaction in porous catalysts using a random three-dimensional network model, *Chem. Eng. Sci.*, 47 (1992) 1761–1770.
- [9] A.O. Imdakm and M. Sahimi, Computer simulation of particle transport processes in flow through porous media, *Chem. Eng. Sci.*, 46 (1991) 1977–1993.
- [10] W.M. Lu and S.C. Ju, *Sep. Sci. Technol.*, 24 (1989) 517.
- [11] K. Stamatakis and C. Tien, A simple model of cross-flow filtration based on particle adhesion, *AIChE J.*, 39 (1993) 1292–1302.
- [12] H.E. Rose and J.E. English, 51 (1973) 14.